


Enabling *Ab Initio* Material Design of InAs/GaSb Superlattices for Infrared Detection

Shengxin Yang¹,[✉] Xiaobi Wang,² Yongfeng Liu,² Jia Wu,² Wenhong Zhou,² Xiangshui Miao,¹ Li Huang,^{2,†} and Kan-Hao Xue^{1,*}

¹Wuhan National Laboratory for Optoelectronics, School of Optical and Electronic Information, Huazhong University of Science and Technology, Wuhan 430074, China

²Wuhan Guide Infrared Co. Ltd., Wuhan 430070, China

 (Received 7 January 2022; revised 10 June 2022; accepted 18 July 2022; published 22 August 2022)

Type-II superlattices (T2SLs) exemplified by InAs/GaSb are promising for infrared detection as the cutoff wavelength can simply be tuned by the layer thickness. Computational material design is thus highly desirable, but traditional methods such as tight binding and $k\cdot p$ depend on the choice of parameters. *Ab initio* density-functional-theory (DFT) calculations, on the other hand, suffer from a dilemma because band-gap accuracy and computational efficiency cannot be reached simultaneously due to band-gap underestimation. Here we show the great potential of the shell DFT-1/2 method in the material design of T2SLs. With a single parameter input, the lattice constant, or even without parameter, the method yields satisfactory electronic structures for a series of InAs/GaSb T2SLs considering spin-orbit coupling, with the band-gap mismatch limited to 5% compared with our industry-class samples. Detailed miniband analysis is presented based on the *ab initio* results. For covalent semiconductors without strong correlation, shell DFT-1/2 proves to be an excellent candidate for accurate band-structure calculation with local-density-approximation-level efficiency. It enables the material design of III-V superlattice materials at the engineering level without introducing empirical parameters.

DOI: [10.1103/PhysRevApplied.18.024058](https://doi.org/10.1103/PhysRevApplied.18.024058)

I. INTRODUCTION

Infrared (IR) detectors are widely used in safeguard, medical care, and military applications [1,2]. Among high-performance cooled IR detectors, (Hg, Cd)Te has been the mainstream commercial technique [3]. Nevertheless, large dimension substrate for (Hg, Cd)Te IR detectors is still difficult to obtain [4]. In contrast, a type-II superlattice (T2SL) IR detector [5,6] made of III-V semiconductors is a very promising alternative with lower costs, fitting mid-wave and long-wave IR detection. GaSb, InAs, AlSb and certain ternary antimonides possess very similar lattice constants, leading to the classic 6.1 Å-family III-V semiconductor superlattices [5]. In typical InAs/GaSb T2SLs, the conduction-band electrons are concentrated in the InAs layers while the valence-band holes are located within the GaSb layers. The carrier separation behavior tends to suppress the Auger recombination and to reduce the dark current [7]. However, the electron and hole bands will penetrate into adjacent layers, forming the minibands. Therefore, the band gap of an InAs/GaSb T2SL is usually lower than that of bulk InAs and bulk GaSb. A great

convenience arises that the target IR wavelength can be tuned by the layer thickness, typically InAs thickness, without altering other technical parameters. This enables tremendous material-design flexibilities, and theoretical calculation is a powerful technique for designing the T2SL materials upon the need of the IR wavelength.

In previous works, empirical methods, such as empirical tight binding [8,9] and $k\cdot p$ models [10–12] have been widely used. Although computationally efficient, the accuracy of these empirical methods actually depends on the selection of experimental data, and it is difficult to account for defects and various interfacial structures under the tight binding or $k\cdot p$ perturbation frameworks. On the other hand, first-principles calculations using density-functional theory (DFT) [13,14] should be a natural approach to enable a broad range of material design for T2SL IR detectors. Unfortunately, the Kohn-Sham *ansatz* does not enable a direct physical meaning of the electron energy eigenvalues, and the obtained “band gap” is, in general, severely lower than the experimental excitation energy [15–17]. For T2SL calculation, this leads to two extremes. In some works, empirical band-gap correction techniques were used based on local-density-approximation (LDA) [14] or generalized-gradient-approximation (GGA) [18–20] calculations [21].

*xkh@hust.edu.cn

†guidehl@163.com

In others, advanced techniques such as the quasiparticle approach [22] within the GW approximation were adopted [23]. Both approaches suffer from certain drawbacks. In the former, empirical input is unavoidable, while for the latter the heavy computational load is a primary concern. The ideal solution is of course a parameter-free *ab initio* calculation method whose computational load is yet at the same level as LDA and GGA. Moreover, experimental data with industrial precision are also required for a proper benchmark of the computational method.

II. METHOD OF BAND-GAP CORRECTION

Fortunately, the 6.1-Å family semiconductors are all normal s - p covalent semiconductors without strong electron correlation, therefore the independent-particle approximation picture is still sufficiently good. A compelling solution is to keep the LDA and GGA correlation (which is, however, the local, dynamical correlation in quantum chemistry [24]), but introduce some nonlocal exchange, like the hybrid functional approach [25]. The key is to rectify the exchange energy, a major proportion of which counteracts the spurious electron self-interaction [26]. The insufficient removal of electron self-interaction causes unphysical strong repulsion for the electrons in the filled valence band, raising the valence band with respect to the conduction band for semiconductors (i.e., band-gap underestimation) [27]. The self-interaction correction (SIC) technique [28] could improve the semiconductor band gaps, but is difficult to implement for covalent compounds. On the other hand, calculating the truly non-local Hartree-Fock exchange, no matter whether in the screened form or not, greatly increases the computational complexity.

Intrinsically, the band-gap problem of DFT persists under LDA and GGA because the fundamental gap of a semiconductor involves not only an N -electron system, but also its ionized $(N-1)$ - and $(N+1)$ -electron counterparts. Hence, the quasiparticle approach [22] is the suitable tool. However, if one does not refer to the expensive GW method, there are other well-accepted explanations to the band-gap problem in DFT, which are intrinsically related to the perspective of SIC. The exact total energy of a ground-state system, with no spurious self-interaction, should vary in a piecewisely linear manner with respect to the electron number [29], provided that fractional occupation is allowed. In this way, the exchange-correlation (XC) energy functional should exhibit some derivative discontinuity when passing through an integral number of electrons, but practically used LDA and GGA XC functionals do not possess derivative discontinuity, rendering the underestimation of band gaps for semiconductors and insulators. In recent years, Koopmans-compliant functionals have been proposed by the Marzari group [30], based on the generalized Koopmans' theorem proved by Dabo

et al. [31]. Koopmans-compliant functionals extend the constraint of piecewise linearity of the total energy to each fractional orbital occupation, thus they are orbital dependent.

On the other hand, keeping the Kohn-Sham framework, Ferreira and coworkers extended the half-occupation technique of Slater to modern DFT calculations in 2008 [32], proposing the DFT-1/2 method. The basic principle of DFT-1/2 is the following discovery:

$$E_{\text{total}}(0) = E_{\text{total}}(-1) + \varepsilon_i \left(-\frac{1}{2} \right), \quad (1)$$

where $E_{\text{total}}(0)$ and $E_{\text{total}}(-1)$ are the total energies of the semiconductor in its ground state and its ionized state with one hole introduced, respectively. Here $\varepsilon_i(-1/2)$ represents the energy eigenvalue for the valence-band maximum (VBM) when the system is deprived of half an electron. It is related to the nominal Kohn-Sham eigenvalue of VBM, $\varepsilon_i(0)$ from the neutral system, through

$$\varepsilon_i \left(-\frac{1}{2} \right) = \varepsilon_i(0) - S_i. \quad (2)$$

Now S_i is a non-negative self-energy-like term that measures how the hole, introduced by intrinsic excitation, deviates from an ideal Bloch state. Since the effect of S_i is to enlarge the band gap, taking into account a non-null S_i is like adding the derivative discontinuity of the XC, according to Ferreira *et al.* [33]. On the other hand, the necessity of considering S_i is justified by the need to overcome the spurious electron self-interaction. Under LDA and GGA, the exchange part of the XC does not exactly cancel the spurious electron self-interaction. The subtraction of S_i aims at removing such a self-interaction term to yield reasonable band gaps, thus lowering the valence-band energy. To sum up, the evaluation of S_i lies at the heart of DFT-1/2.

While the detailed expression of S_i is complicated [32,33], there is a convenient way to derive it without referring to the quasiparticle equations, according to DFT-1/2. As the hole is usually localized on a particular atom (or sometimes shared by two adjacent atoms), it is assumed that S_i can be transferred to a solid using the reference atomic calculation results [32]. A so-called self-energy potential is first derived from the all-electron DFT calculations for an atom, which is then summed up to the pseudopotential of the corresponding element in the solid. As the Coulomb-type potential is long-range in nature, the self-energy potential has to be trimmed before its introduction to solid-state calculations. The cutoff radius (r_{cut}) is obtained in a variational way as to maximize the band gap, which corresponds to the minimization of the ground-state energy in its neutral state. Hence, r_{cut} is not empirical and is determined by variation, and DFT-1/2 is free of empirical parameters.

The computational load of DFT-1/2 is merely at the LDA and GGA level, but it yields accurate band gaps for many semiconductors and insulators [33,34]. A great flexibility of DFT-1/2 lies in that it does not generate the correct total energy and electronic structure at the same time. Rather, its geometric optimization and total energy calculation rely on the LDA and GGA runs, which are however quite satisfactory in general. The electronic structures are derived through a post run with self-energy correction, but carried out in real space in order to save the computational load. Hence, DFT-1/2 performs extremely well in terms of convergence, and the transferability of self-energy-corrected pseudopotentials enables straightforward calculations for larger supercells.

Nevertheless, when applied to covalent semiconductors, DFT-1/2 still suffers from band-gap inaccuracy and uncertainty for the charge-stripping strategy [35]. Figure 1 illustrates the most probable spatial locations for the valence-band hole and conduction-band electron in a III-V semiconductor GaSb. Since the holes are localized near the Sb anions [Fig. 1(a)], a tentative spherical region may be suitable for the application of the self-energy potential. However, Fig. 1(b) indicates that the electron in the conduction band also possesses a high probability to emerge near the Sb anions, though another highly probable region is surrounding the Ga cations. In this case, DFT-1/2 suffers from an artificial downshift of the conduction band, which is not only improper but also uncontrollable. A shell-correction extension, shell DFT-1/2, was further suggested in 2018 by one of the authors [36], which works well for covalent semiconductors such as Ge and III-V compounds. Shell DFT-1/2 involves two cutoff radii (r_{in} and r_{out}), both should be optimized to yield a maximum band gap. The key fact is that the hole in the valence band is usually shared by the two atoms forming the bond, and the conduction-band electron may have a considerable probability to emerge in the near-core regions. Hence, the skipping of an inner sphere in the self-energy potentials is usually useful for not disturbing the conduction band of covalent semiconductors. In this sense, we claim

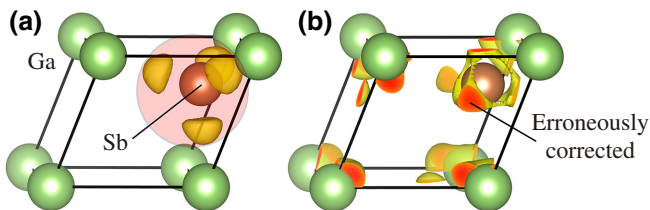


FIG. 1. (a) The most probable spatial regions of the hole in GaSb, where the red circle denotes a tentative spherical region to cover the hole location. (b) The most probable spatial regions of the electron in GaSb, showing the spurious correction for the conduction band since the electron has a high possibility to emerge in that red sphere.

that shell DFT-1/2 does not include corrections based on DFT-1/2. Rather, it is a method that strives to minimize the unexpected corrections, which may be erroneously applied to the conduction band. This can be very helpful for covalent semiconductors. The limitation of shell DFT-1/2 lies in that it still relies on a real-space filter to discriminate the hole from the electron. In certain cases like Li_2O_2 [36] and Cu_2O [35], which involve intermediate valency of some elements (O^- in Li_2O_2 and Cu^+ in Cu_2O), this method fails because the hole and the electron are entangled in the same shell-like region of the real space. However, for strongly covalent III-V semiconductors, the carrier distribution resembles that of Fig. 1, and a shell region can indeed effectively cover the hole-localization regions.

In this work, we show that the shell DFT-1/2 method is a proper solution for the materials design for T2SL IR detectors, in that it enables *ab initio* calculations without empirical parameter input, or only with a lattice constant input. The electronic structures of a series of InAs/GaSb T2SLs are investigated using shell GGA-1/2 (shGGA-1/2), which are compared with our experiments to verify the accuracy.

III. EXPERIMENT

Six photodiode structures are grown in a solid-source molecular beam epitaxy (MBE) system. The 50-mm-size epi-ready *n*-type GaSb (001) wafers are utilized, with Te doping. After oxide desorption, approximately 300-nm-thick GaSb buffer and approximately 3- μm superlattice are deposited. The structure consists of a 0.5- μm -thick *p*+ contact layer, a 2- μm -thick slightly *p*-doped π region with constant doping concentration, a 0.5- μm -thick *n*+ region, and topped with a 0.01- μm -thick InAs:Si *n*+ doped contact layer. The photodiode structure is schematically shown in Fig. 2(a). The superlattices are composed of alternating thin layers of InAs and GaSb with a period thickness of 46 to 72 Å. All samples are processed and characterized in exactly the same way, using standard wet-etching techniques. The devices are not passivated or antireflection coated. After device fabrication, strain-balanced *x* monolayer (ML) InAs/0.1*x* ML InSb/*y* ML GaSb T2SL samples are investigated using X-ray diffraction (XRD). The precise lattice-matched composition is determined from coupled $\omega - 2\theta$ XRD scans from the (004) planes in a series of calibration samples. Finally, for optical absorption measurement, the wavelengths of the photodetectors are measured by Fourier transform infrared (FTIR) spectroscopy.

As shown in Table I, the X-ray peak full widths at half maximum (FWHM) of all samples are controlled to within 50 arcs and the mismatches are controlled to within 1000 ppm, indicating high material quality. The structural properties of the superlattices are determined using

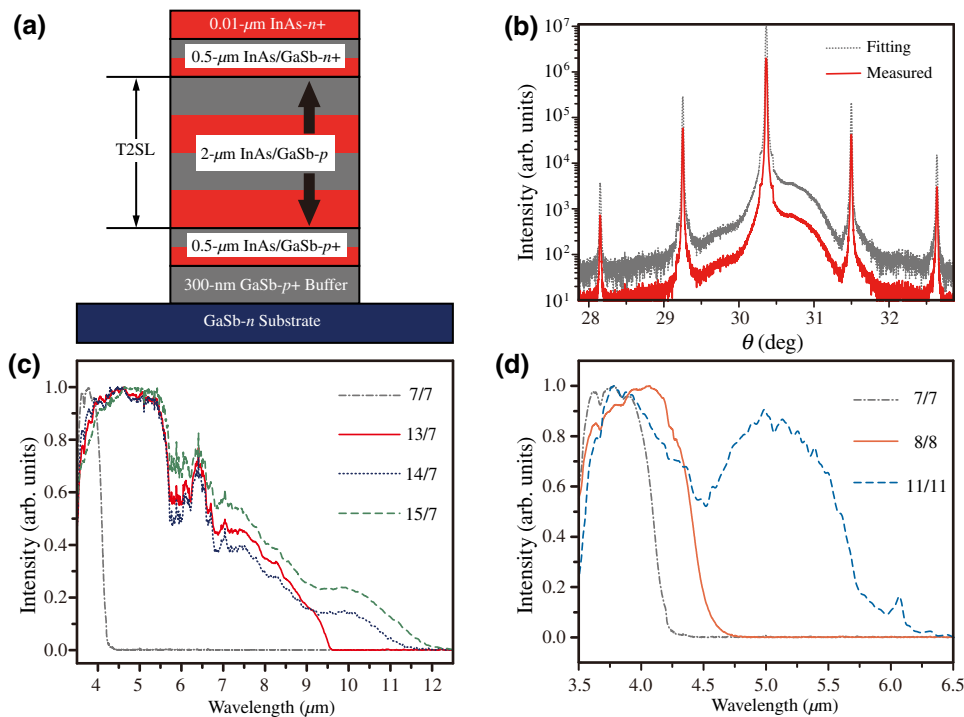


FIG. 2. (a) Illustration of the photodiode structure. (b) Simulation of high-resolution XRD rocking curve of a typical sample (sample A). (c) FTIR spectroscopy results for samples A–D. (d) FTIR spectroscopy results for samples A, E, and F.

commercial dynamical XRD software X’pert Epitaxy and a self-consistent analysis of coupled $\omega - 2\theta$ XRD scans of each sample. In this analysis, the satellite-peak spacing determines the composition of InAs and GaSb. This conventional approach to modeling the XRD data yields the set of structural parameters shown in Table I, confirming that the structures of the as-grown samples are consistent with our design. The fitted high-resolution XRD rocking curve of sample A is shown in Fig. 2(b). From the substrate-peak spacing, the in-plane lattice constant of GaSb is measured to be approximately 6.096 Å. The experiments demonstrate the flexibility in band-gap tuning of the T2SLs, as demonstrated in the FTIR measurement results shown in Figs. 2(c) and 2(d). The slight oscillations in Figs. 2(c) and 2(d) are due to a poor signal-to-noise ratio, which is related to various factors including the absorbing layer thickness, device structure, doping, and so forth. The 0% cutoff wavelengths of various compositions of the T2SL are given in Table II, where the corresponding band-gap values can readily be derived.

IV. CALCULATIONS AND ANALYSIS

As single-crystal GaSb serves as the substrate, in our superlattice calculations the a - and b -axis lattice constants are fixed to the experimental value 6.096 Å for all T2SL models. The PBEsol functional [37], which typically yields accurate lattice constants, is adopted for the exchange-correlation energy for minimizing the residue stress. The calculations are carried out using Vienna *ab initio* simulation package (VASP 5.4.4) [38,39] with the projector augmented-wave method [40,41], and the

plane-wave basis is truncated at a 250-eV kinetic energy cutoff. Spin-orbit coupling is considered in all electronic structure calculations. For GGA we attempt PBE [20], PBEsol [37], and AM05 [42] functional forms. For bulk InAs and GaSb, a $25 \times 25 \times 25$ Γ -centered equal-spacing k -point mesh [43] is used to sample the Brillouin zones. Detailed computational parameters and convergence test results are given in Note S1 within the Supplemental Material [56].

We first examine the accuracy of various methods in calculating the electronic band structures of GaSb and InAs. To this purpose, the optimized lattice constant through calculation is adopted. As prototype zinc-blende semiconductors with two atoms per primitive cell, the GGA and shell GGA-1/2 band structures could be compared with the Heyd-Scuseria-Ernzerhof (HSE06) hybrid functional [44,45] calculation results all with spin-orbit coupling, as illustrated in Fig. 3. In shell GGA-1/2, the strong covalent nature of GaSb and InAs requires the implementation of shGGA-1/4-1/4, where the first and second 1/4 stand for 1/4 electron removal for III and V elements, respectively. The inner and outer self-energy potential cutoff radii for both III and V elements are obtained in a variational way to maximize the band gap. This is because the recovered ground state, through hole filling, must be in an energy minimum, as explained in the original work of Ferreira *et al.* [32]. Figures 3(a) and 3(d) show that GGA-PBEsol predicts no band gap for both semiconductors, and the degeneration relations among the p -orbital valence bands are also different from the normal spin-orbit coupling splitting, in sharp contrast to experimental facts. The HSE06 results are much improved, though the

TABLE I. Structural properties of experimental samples.

Sample	Structure	Period thickness (Å)	Mismatch (ppm)	FWHM (arcsec)	
				Diffraction peak on rocking curve	−1st diffraction peak on $\omega-2\theta$ curve
A (7/7)	7.23 ML InAs/0.71 ML InSb/7.02 ML GaSb	46.3	0	50.73	49.65
B (13/7)	13.00 ML InAs/1.30 ML InSb/6.99 ML GaSb	65.9	0	43.21	42.23
C (14/7)	14.03 ML InAs/1.39 ML InSb/6.99 ML GaSb	67.6	−368	33.62	31.89
D (15/7)	14.98 ML InAs/1.48 ML InSb/6.98 ML GaSb	71.4	0	41.32	40.72
E (8/8)	8.06 ML InAs/0.74 ML InSb/8.06 ML GaSb	52.1	−654	37.22	38.63
F (11/11)	11.10 ML InAs/1.11 ML InSb/11.09 ML GaSb	71.0	0	41.98	41.70

predicted band gaps (0.57 eV for GaSb, 0.22 eV for InAs) are still noticeably smaller than experimental values (0.81 eV for GaSb, 0.42 eV for InAs). In contrast, shGGA-1/4-1/4 yields a 0.83-eV gap for GaAs and a 0.58-eV gap for InAs, better fitting the experimental data. Our calculated InAs gap is larger than experiment, which however also frequently occurs in *GW* calculations. Certain techniques may be applied to tune the InAs gap to experiment, such as adjusting the strength of In and As self-energy potentials. Nevertheless, this goes against the spirit of *ab initio* calculations, and in this work we stick to the original electronic structure of shGGA-1/2 without introducing any empirical parameter.

The computational load of a single shGGA-1/4-1/4 run is actually at the same level of GGA [36], though several trial runs should be conducted on the two-atom primitive cells. The optimum cutoff radii for In, As, Ga, and Sb as listed in Table III are, however, transferable to other calculations, thus there is no need to rescan these radii in T2SL calculations. The overall high quality of shGGA-1/4-1/4 band structures for bulk GaSb and InAs, without empirical parameters, promise their application potential in superlattices. It is worthwhile to note that the GGA-1/2 gap for InAs (0.85 eV) is even larger than GaSb (0.70 eV), and both gap values do not fit experimental well. This reveals that it is only shell DFT-1/2, rather than standard DFT-1/2, that performs well for III-V semiconductors like InAs and GaSb.

TABLE II. Optical measurement results for the six samples.

Sample	Peak (μm)	Cutoff Wavelength (μm)		
		50% cutoff	10% cutoff	0% cutoff
A	3.79	4.09	4.20	4.40
B	4.66	7.04	9.34	9.53
C	5.20	6.75	10.58	11.72
D	5.34	7.65	11.22	12.44
E	4.06	4.41	4.56	4.75
F	3.77	5.57	6.10	6.37

While there are numerous compositions for InAs/GaSb T2SLs, our primary composition is a T2SL consisting of 7 MLs of GaSb and 7 MLs of InAs, here denoted as the 7/7 model. Other compositions of InAs/GaSb T2SL models are discussed in detail in Note S2 within the Supplemental Material [56]. For detailed supercell information, we attach the model structural files (VASP POSCAR format) in a separate zip file [57]. Figure 4(a) illustrates the 7/7 atomic model structure. The minibands in T2SLs account for the fundamental gap, which has been well accepted and supported by calculations [46–48]. However, there is a lack of *ab initio* calculations to unambiguously support or criticize this picture. To construct a 7/7 model that is most close to experimental structure, one has to consider the exact interfacial atomic arrangement. Our model can be denoted by 7 ML InAs/0.7 ML InSb/7 ML GaSb, where the formation of 0.7 ML InSb is due to the two 0.35 ML InSb layers belonging to GaSb and InAs, respectively. However, as the As source persists during our fabrication, these two layers possess a stoichiometry of InAs_{0.65}Sb_{0.35}, as enclosed by a red box in Fig. 4(a). In order to ensure the As : Sb atomic ratio to be approximately 0.65:0.35, we enlarge the T2SL supercell to 2×2 along the $a-b$ plane, where each ML contains eight In atoms, five As atoms, and three Sb atoms. Therefore, the As : Sb ratio in our model is 0.625:0.375, which is quite close to experiment. The shGGA-1/2 calculation on the T2SL requires applying the self-energy potentials of In, As, Ga, Sb all subject to 1/4 electron removal, with the cutoff radii specified in Table III. For comparison, we also carry out GGA calculations using the PBEsol functional.

A remarkable benefit of the shGGA-1/2 method is that the opening of the band gap allows us to analyze the minibands of T2SLs in detail. It is well accepted that the electrons and holes of InAs/GaSb T2SLs are spatially separated, with the former constrained in the InAs layer while the latter located in the GaSb layer. The shGGA-1/2 electronic structure analysis for the 7/7 model is given in Figs. 4(b)–4(f). The nonempirical calculation shows that the VBM state is surrounding the Sb atoms in real space, while the

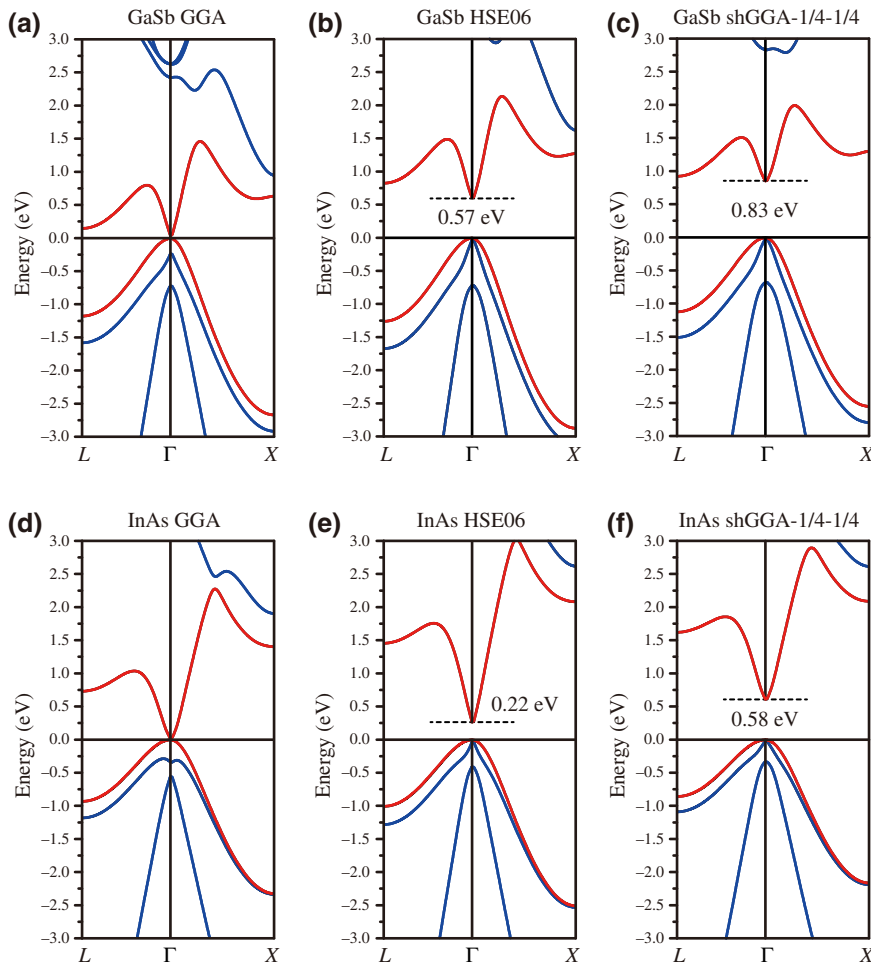


FIG. 3. Electronic band structures of bulk III-V semiconductors. (a) GaSb by PBEsol; (b) GaSb by HSE06; (c) GaSb by shGGA-1/4-1/4; (d) InAs by PBEsol; (e) InAs by HSE06; (f) InAs by shGGA-1/4-1/4. All calculations consider spin-orbit coupling.

conduction-band minimum (CBM) is close to both In and As atoms in the InAs layer. Moreover, the CBM locations are close to the central InAs region, but the VBM well extends to the interfacial regions. Electronic band structures calculated using shGGA-1/2 and GGA are compared in Figs. 4(e) and 4(f). The GGA-PBEsol band gap is very tiny and is an indirect one, in contrast to experimental results. On the other hand, shGGA-1/2 gives a direct band gap of 271 meV, corresponding to 4.576- μm wavelength. The mismatch to experiment (4.4 μm) is merely 4%. On the other hand, the energy splitting between the first heavy-hole band (HH_1) and the light-hole band (LH_1) at the Γ point ($\text{HH}_1\text{-LH}_1$) is 129 meV

according to our shGGA-1/2 calculation [Fig. 4(e)]. While the conduction band shows prominent dispersion for both in-plane and c directions, HH_1 has almost no dispersion along the c direction.

Our results further confirm the existence of minibands in InAs/GaSb T2SLs and their relative levels in energy determine the band gap. The quantum confinement effect is of course relevant to the well width, thus the band gap can be tuned through adjusting the layer thickness. In Note S3 within the Supplemental Material [56], we analyze charge distributions at the Γ point of more bands around the band gap, and identify eight minibands out of the nonminibands. Our shGGA-1/2 calculations do not involve empirical

TABLE III. Optimal shGGA-1/4-1/4 self-energy potential cutoff radii for GaSb and InAs and the corresponding band gaps.

III-V Material	Self-energy potential cutoff radii (Bohr)				Band gap (eV)			
	III element		V element		HSE06	GGA-1/2 ($n=20$)	shGGA-1/2	Expt.
	r_{in}	r_{out}	r_{in}	r_{out}				
GaSb	2.2	4.0	1.7	3.6	0.57	0.70	0.83	0.81
InAs	2.4	4.5	1.4	3.5	0.22	0.75	0.58	0.41

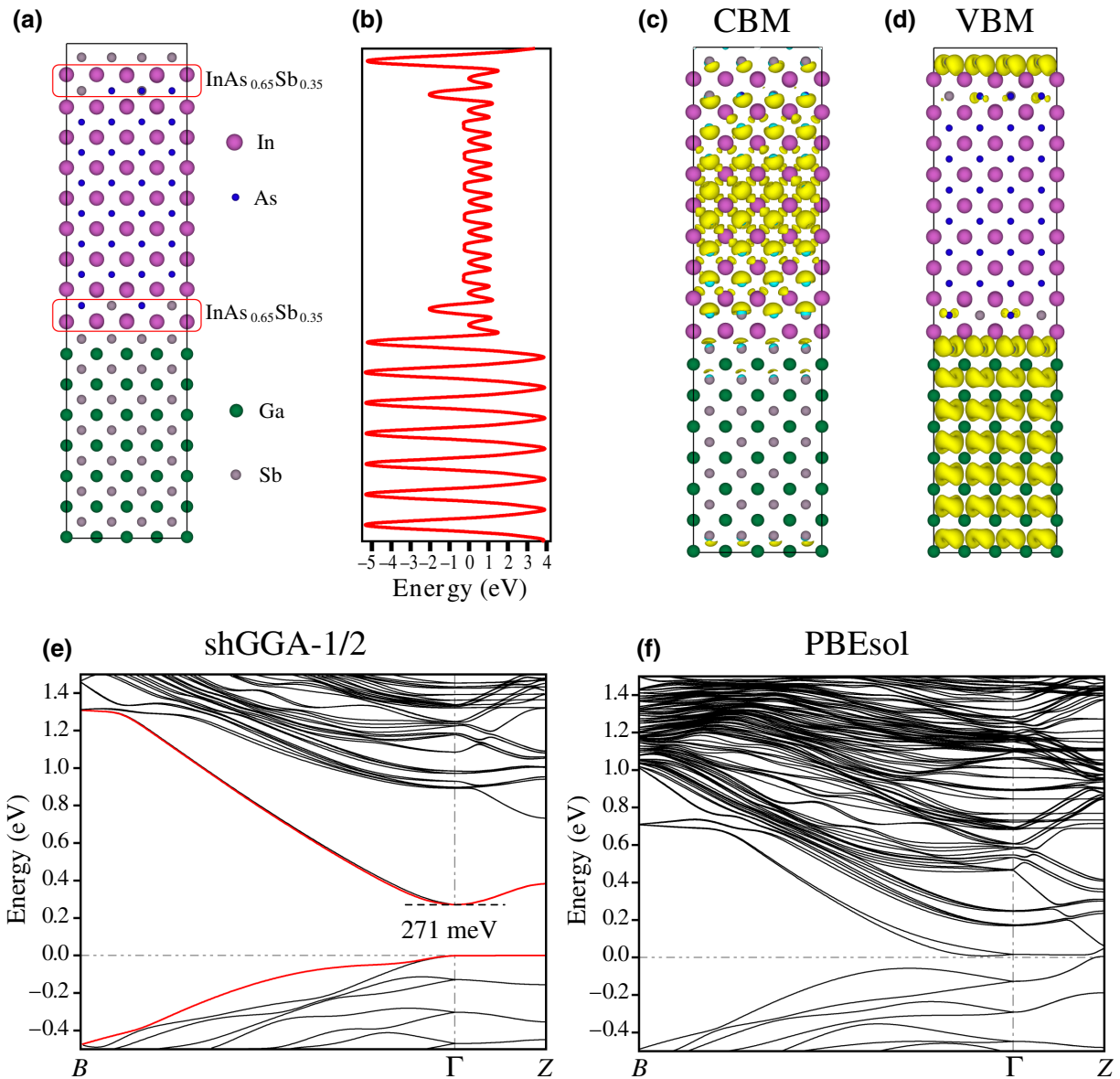


FIG. 4. (a) Atomic structure of our 7 ML InAs/0.7 ML InSb/7 ML GaSb model supercell. (b) Its planar averaged Hartree potential vertically aligned with the supercell. (c) Spatial distribution of the electronic state at the conduction-band minimum (CBM). (d) Spatial distribution of the electronic state at the valence-band maximum (VBM). (e) The electronic band structure calculated using shGGA-1/2. (f) The electronic band structure calculated using GGA-PBESol.

parameters, thus we have to stick to the exact outcomes for bulk InAs and GaSb band structures. The shGGA-1/2 band gap for InAs is 0.58 eV, larger than experimental value (extrapolated to zero temperature) 0.41 eV. In fact, 0.58 eV is already a rather good result among nonempirical *ab initio* calculations, but it does not reach engineering accuracy, even considering the possible exciton effect in experimental measurement. The mismatch is 0.17 eV, or approximately 40% because InAs is a narrow-gap semiconductor. However, the band gap for the T2SLs stems from excitation between minibands, which reflects

a quantum confinement effect that can be well described by DFT calculations. Hence, the theory-to-experimental mismatch on the InAs fundamental gap has been alleviated because one is more concerned with the positions of the minibands that are specific to the superlattice structure. The overall shGGA-1/2 gap prediction error for the T2SL does not exceed 5%.

Up to now we have not included the 3*d* (4*d*) electrons of Ga (In) in the valence, as such tends to greatly increase the computational cost. However, these electrons are semicore electrons and may influence the electronic

structure of the semiconductor, though to a less extent in covalent bonding. To explore the possible impact of these semicore d electrons, we include them in the valence and the corresponding shGGA-1/2 electronic structures for several T2SLs are given in Note S6 within the Supplemental Material [56]. Compared with the results that treat these d electrons in the core, the maximum band-gap discrepancy is merely 14 meV. And compared with experimental values, the maximum band-gap mismatch is approximately 15 meV when these d electrons are included in the valence. Therefore, the impact of the d shell is minor and can be neglected in the calculations.

In considering the practical growth, we establish another model for 7/7 (model β , cf. Note S4 within the Supplemental Material [56]), where the model in Fig. 4(a) will be referred to as model α). As shown in Fig. S4(a) within the Supplemental Material, its 0.7 ML no longer consists of two $\text{InAs}_{0.65}\text{Sb}_{0.35}$, but rather $\text{In}_{0.35}\text{Ga}_{0.65}\text{Sb}$ and $\text{InAs}_{0.65}\text{Sb}_{0.35}$, and the atomic structure of model β is illustrated in Fig. S4(b) within the Supplemental Material. The electronic structure of model β is also calculated using GGA-PBEsol and shGGA-1/2, where the band gap of the former is merely 10 meV, which is indirect. The predicted band gap for model β is 293 meV using shGGA-1/2, which is approximately 3.9% larger than our experimental value and lower than that of model α . Band-structure details are given in Fig. S4(c) within the Supplemental Material. The difference between model α and model β in terms of the band gap is minor.

Using model α , we further study the influence of InAs thickness on InAs/GaSb T2SLs, by fixing GaSb to 7 ML. The number of layers for InAs (x) is scanned from 3 to 15 with an interval of 2. The interfacial layer configuration is 0.1x ML InSb. Figure 5(a) illustrates the variation of band gap as well as the energy splitting $\text{HH}_1\text{--LH}_1$ with respect to x . Band gap decreases sharply when InAs goes thicker, consistent with our expectation, but the speed of decrease is lower for high x values. Meanwhile, $\text{HH}_1\text{--LH}_1$

decreases as well, but in a mild manner. The calculated band-gap values match the experimental results with 7/7, 13/7, 14/7, and 15/7 compositions quite well. On the other hand, we also studied model α for equal-layer InAs/GaSb, i.e., x ML InAs/0.1x ML InSb/ x ML GaSb with $x=7, 8, 11$ and 12. The band gaps are consistent with experimental values as shown in Fig. 5(b). Nevertheless, in this case the degradation of band gap with x is increasingly fast for large x . $\text{HH}_1\text{--LH}_1$ also decreases monotonously, and the rate of decrease is slower for large x . The band structures of all models other than 7/7 in Fig. 5 are shown in Fig. S2 within the Supplemental Material.

The tight-binding method (TBM) is a celebrated approach in solid-state physics, and has been widely applied to Sb-based T2SL calculations. Wei and Razeghi prescribed the detailed parameters for InAs/GaSb superlattices using tight binding [49]. We therefore calculated all the superlattice systems in Fig. 5 that are subject to shGGA-1/2 calculations, using tight binding and the parameters from Wei and Razeghi [49]. This approach requires fixing the elemental composition of each layer. Knowing the elemental proportion of the local layer and that of the adjacent layers, a weighted averaging would yield the strains due to elemental mixing. Here only the strains along the [001] direction matter, thus the elastic constants c_{11} and c_{12} are required. We adopt the values from the CRC Handbook of Chemistry and Physics [50]. The efficiency of tight binding is extremely remarkable, such that we can adopt the exact compositions for the interface. For instance, in 7 ML InAs/0.7 ML InSb/7 ML GaSb, the interfacial layer is set to $\text{InAs}_{0.65}\text{Sb}_{0.35}$, instead of $\text{InAs}_{0.625}\text{Sb}_{0.375}$ that is adopted in DFT calculations. In standard TBM calculations, the supercell structure literally follows the experimental lattice constants as well as the zinc-blende structure. For parameterized-TBM calculations, the supercell structures are kept the same as that in shDFT-1/2 calculations, but the Slater-Koster parameters follow that of Wei and Razeghi.

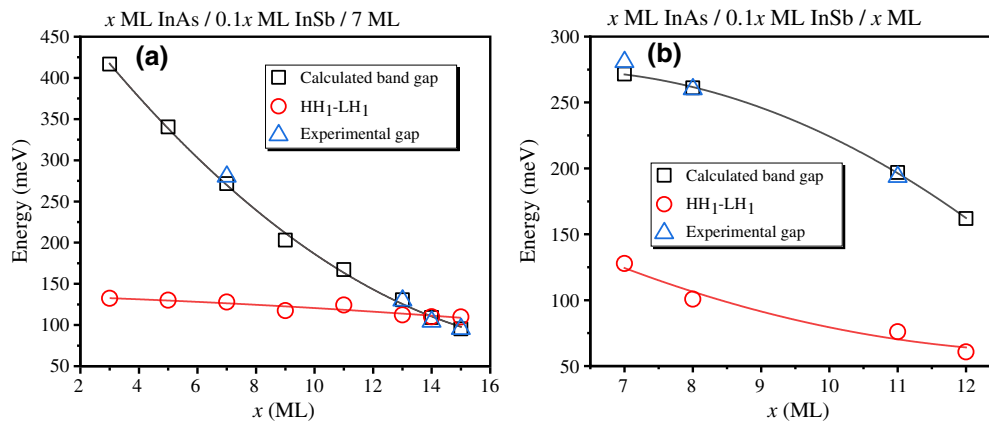


FIG. 5. Band gaps and $\text{HH}_1\text{--LH}_1$ values for (a) x ML InAs/0.1x ML InSb/7 ML GaSb; (b) x ML InAs/0.1x ML InSb/ x ML GaSb.

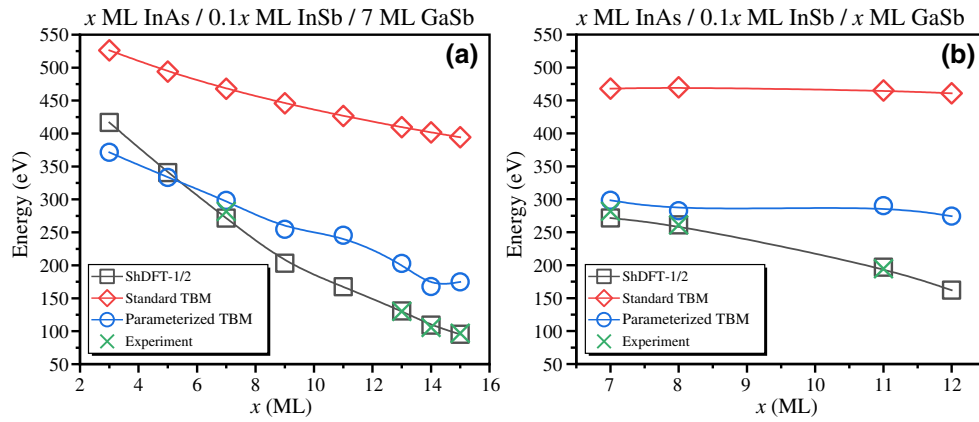


FIG. 6. Band gaps calculated by standard TBM, parameterized TBM and shDFT-1/2 with reference to experimental values, for (a) x ML InAs/0.1x ML InSb/7 ML GaSb; (b) x ML InAs/0.1x ML InSb/ x ML GaSb.

Figure 6 demonstrates a comparison of T2SL band gaps between standard TBM, parameterized TBM as well as shDFT-1/2 results, with reference to experimental values. It is observed that the overall tight binding band gaps are larger than experiment, and the slope with respect to x is not as steep as the experimental curve. The average mismatch to experiment is 200–300 meV.

Besides TBM, we also compare shDFT-1/2 with another efficient rectification method, based on DFT LDA and proposed by Wang *et al.* [51,52] (details shown in Note S7 within the Supplemental Material [56]). Both based on the experimental superlattice information by Ongstad *et al.* [53,54], the maximum absolute errors in shGGA-1/2 and the method by Wang *et al.* are similar (8.6% in the former and approximately 10% in the latter). The major benefit of shGGA-1/2, of course, lies in that it does not involve empirical parameters and is thus supposed to fit a broader scope of materials. In addition, we also benchmark shGGA-1/2 against a state-of-the-art metaGGA functional, the strongly constrained and appropriately normed (SCAN) functional [55]. The model- α structures of 7 ML InAs/0.7 ML InSb/7 ML GaSb as well as 8 ML InAs/0.8 ML InSb/8 ML GaSb are selected. Unfortunately, the SCAN calculation results do not open a band gap for these T2SL models, which is inconsistent with the experimental results. Detailed SCAN calculations are given in Note S8 within the Supplemental Material [56].

It deserves to also explore the situation where no parameter is permitted in the calculation, including the lattice constant. Then the a/b lattice constant can be taken as the optimized GaSb (serving as the substrate) lattice constant, which is 6.128 Å. The band gaps calculated for 7/7 model α and model β are both 297 meV, which are approximately 5.4% larger than the experimental value

(more details given in Note S5 within the Supplemental Material [56]). Hence, even fully *ab initio* calculation, involving no experimental parameters, could render satisfactory results, and the minor mismatch may be attributed to the slight inaccuracy due to lattice-constant prediction. And the computational load of shGGA-1/2 is kept acceptable. The maximum supercell of this work involves approximately 350 atoms, for which a self-consistent run plus energy band-diagram calculation, all with spin-orbit coupling, costs around 80 h on a 48-core computer.

The application of DFT has not been so popular in electronics compared with chemistry. Indeed, if nonempirical DFT is not only more computational demanding, but also with much worse band-gap prediction, then its *ab initio* benefit with respect to tight binding is not so attractive. Nevertheless, efficient band-gap correction methods like shell DFT-1/2 are highly useful and we envisage that the application of DFT can grow fast in the semiconductor industry with the ever-increasing computational power. If strongly correlated compounds are involved, such as 3d transition metal oxides, then the shell DFT-1/2 correction can be carried out based on a DFT + U ground state, which is still much more efficient than hybrid functional or *GW*.

In conclusion, the self-energy corrected shell DFT-1/2 method is shown to yield accurate band structures for a series of InAs/GaSb T2SLs, consistent with our optical measurement results, demonstrating less than 5% mismatch in the band gap. The miniband structures for the superlattices are revealed. By fixing the GaSb layer thickness, we demonstrate the trend of sharp band gap decrease through increasing the InAs layer thickness. Also, by equaling the number of layers (x) for InAs and GaSb, the superlattice band gap goes down when x increases, and the rate of gap decay is much faster at large x values. The shell DFT-1/2 method together with the PBEsol functional

is promising for *ab initio* material design for T2SLs, at a GGA-level computational load.

ACKNOWLEDGMENTS

This work is supported by the National Natural Science Foundation of China under Grant No. 61974049.

- [1] A. Rogalski, Recent progress in infrared detector technologies, *Infrared Phys. Techn.* **54**, 136 (2011).
- [2] B. B. Lahiri, S. Bagavathiappan, T. Jayakumar, and J. Philip, Medical applications of infrared thermography: A review, *Infrared Phys. Techn.* **55**, 221 (2012).
- [3] W. Lei, J. Antoszewski, and L. Faraone, Progress, challenges, and opportunities for HgCdTe infrared materials and detectors, *Appl. Phys. Rev.* **2**, 041303 (2015).
- [4] D. Brellier, E. Gout, G. Gaude, D. Pelenc, P. Ballet, T. Miguet, and M. C. Manzato, Bulk growth of CdZnTe: Quality improvement and size increase, *J. Electron. Mater.* **43**, 2901 (2014).
- [5] A. Rogalski, P. Martyniuk, and M. Kopytko, InAs/GaSb type-II superlattice infrared detectors: Future prospect, *Appl. Phys. Rev.* **4**, 031304 (2017).
- [6] F. Bertazzi, A. Tibaldi, M. Goano, J. A. G. Montoya, and E. Bellotti, Nonequilibrium Green's Function Modeling of Type-II Superlattice Detectors and its Connection to Semiclassical Approaches, *Phys. Rev. Appl.* **14**, 014083 (2020).
- [7] Y. Aytac, B. V. Olson, J. K. Kim, E. A. Shaner, S. D. Hawkins, J. F. Klem, J. Olesberg, M. E. Flatté, and T. F. Boggess, Bandgap and temperature dependence of Auger recombination in InAs/InAsSb type-II superlattices, *J. Appl. Phys.* **119**, 215705 (2016).
- [8] V. Sankaran, K. W. Kim, and G. J. Iafrate, Tight-binding study of optical properties in short-period $\text{In}_{0.53}\text{Ga}_{0.47}\text{As}/\text{InP}$ superlattices, *Phys. Rev. B* **53**, 6939 (1996).
- [9] S. Abdollahi Pour, B. Movaghar, and M. Razeghi, Tight-binding theory for the thermal evolution of optical band gaps in semiconductors and superlattices, *Phys. Rev. B* **83**, 115331 (2011).
- [10] Y. Aytac, B. V. Olson, J. K. Kim, E. A. Shaner, S. D. Hawkins, J. F. Klem, M. E. Flatté, and T. F. Boggess, Evidence of a Shockley-Read-Hall Defect State Independent of Band-Edge Energy in InAs/In(As,Sb) Type-II Superlattices, *Phys. Rev. Appl.* **5**, 054016 (2016).
- [11] M. Rygała, K. Ryczko, T. Smółka, D. Kujawa, P. Martyniuk, T. J. Ronningen, S. Krishna, and M. Motyka, Investigating the physics of higher-order optical transitions in InAs/GaSb superlattices, *Phys. Rev. B* **104**, 085410 (2021).
- [12] B. Jogai and D. N. Talwar, Interband optical absorption in strained InAs/In_xGa_{1-x}Sb type-II superlattices, *Phys. Rev. B* **54**, 14524 (1996).
- [13] P. Hohenberg and W. Kohn, Inhomogeneous electron gas, *Phys. Rev.* **136**, B864 (1964).
- [14] W. Kohn and L. J. Sham, Self-consistent equations including exchange and correlation effects, *Phys. Rev.* **140**, A1133 (1965).
- [15] L. J. Sham and M. Schlüter, Density-functional theory of the band gap, *Phys. Rev. B* **32**, 3883 (1985).
- [16] M. Städele, M. Moukara, J. A. Majewski, P. Vogl, and A. Görling, Exact exchange Kohn-Sham formalism applied to semiconductors, *Phys. Rev. B* **59**, 10031 (1999).
- [17] A. J. Cohen, P. Mori-Sánchez, and W. Yang, Insights into current limitations of density functional theory, *Science* **321**, 792 (2008).
- [18] A. D. Becke, Density-functional exchange-energy approximation with correct asymptotic behavior, *Phys. Rev. A* **38**, 3098 (1988).
- [19] J. P. Perdew and Y. Wang, Accurate and simple analytic representation of the electron-gas correlation energy, *Phys. Rev. B* **45**, 13244 (1992).
- [20] J. P. Perdew, K. Burke, and M. Ernzerhof, Generalized Gradient Approximation Made Simple, *Phys. Rev. Lett.* **77**, 3865 (1996).
- [21] W.-F. Sun, M.-C. Li, and L.-C. Zhao, First-principles study of interface relaxation effect on interface and electronic structures of InAs/GaSb superlattices with different interface types, *Superlattices Microstruct.* **49**, 81 (2011).
- [22] L. Hedin, New method for calculating the one-particle Green's function with application to the electron-gas problem, *Phys. Rev.* **139**, A796 (1965).
- [23] Z. Taghipour, E. Shojaei, and S. Krishna, Many-body perturbation theory study of type-II InAs/GaSb superlattices within the GW approximation, *J. Phys.: Condens. Matter* **30**, 325701 (2018).
- [24] A. D. Becke, Density functionals for static, dynamical, and strong correlation, *J. Chem. Phys.* **138**, 074109 (2013).
- [25] A. D. Becke, A new mixing of Hartree-Fock and local density-functional theories, *J. Chem. Phys.* **98**, 1372 (1993).
- [26] P. Mori-Sánchez, A. J. Cohen, and W. Yang, Many-electron self-interaction error in approximate density functionals, *J. Chem. Phys.* **125**, 201102 (2006).
- [27] G.-Q. Mao, Z.-Y. Yan, K.-H. Xue, Z. Ai, S. Yang, H. Cui, J.-H. Yuan, T.-L. Ren, and X. Miao, DFT-1/2 and shell DFT-1/2 methods: electronic structure calculation for semiconductors at LDA complexity, *J. Phys.: Condens. Matter* **34**, 403001 (2022).
- [28] J. P. Perdew and A. Zunger, Self-interaction correction to density-functional approximations for many-electron systems, *Phys. Rev. B* **23**, 5048 (1981).
- [29] E. Kraisler and L. Kronik, Piecewise Linearity of Approximate Density Functionals Revisited: Implications for Frontier Orbital Energies, *Phys. Rev. Lett.* **110**, 126403 (2013).
- [30] G. Borghi, A. Ferretti, N. L. Nguyen, I. Dabo, and N. Marzari, Koopmans-compliant functionals and their performance against reference molecular data, *Phys. Rev. B* **90**, 075135 (2014).
- [31] I. Dabo, A. Ferretti, N. Poilvert, Y. Li, N. Marzari, and M. Cococcioni, Koopmans' condition for density-functional theory, *Phys. Rev. B* **82**, 115121 (2010).
- [32] L. G. Ferreira, M. Marques, and L. K. Teles, Approximation to density functional theory for the calculation of band gaps of semiconductors, *Phys. Rev. B* **78**, 125116 (2008).
- [33] L. G. Ferreira, M. Marques, and L. K. Teles, Slater half-occupation technique revisited: The LDA-1/2 and GGA-1/2 approaches for atomic ionization energies and band gaps in semiconductors, *AIP Adv.* **1**, 032119 (2011).
- [34] J.-H. Yuan, Q. Chen, L. R. C. Fonseca, M. Xu, K.-H. Xue, and X.-S. Miao, GGA-1/2 self-energy correction

- for accurate band structure calculations: The case of resistive switching oxides, *J. Phys. Commun.* **2**, 105005 (2018).
- [35] J. Doumont, F. Tran, and P. Blaha, Limitations of the DFT-1/2 method for covalent semiconductors and transition-metal oxides, *Phys. Rev. B* **99**, 115101 (2019).
- [36] K.-H. Xue, J.-H. Yuan, L. R. C. Fonseca, and X.-S. Miao, Improved LDA-1/2 method for band structure calculations in covalent semiconductors, *Comp. Mater. Sci.* **153**, 493 (2018).
- [37] J. P. Perdew, A. Ruzsinszky, G. I. Csonka, O. A. Vydrov, G. E. Scuseria, L. A. Constantin, X. Zhou, and K. Burke, Restoring the Density-Gradient Expansion for Exchange in Solids and Surfaces, *Phys. Rev. Lett.* **100**, 136406 (2008).
- [38] G. Kresse and J. Furthmüller, Efficient iterative schemes for *ab initio* total-energy calculations using a plane-wave basis set, *Phys. Rev. B* **54**, 11169 (1996).
- [39] G. Kresse and J. Furthmüller, Efficiency of *ab-initio* total energy calculations for metals and semiconductors using a plane-wave basis set, *Comp. Mater. Sci.* **6**, 15 (1996).
- [40] P. E. Blöchl, Projector augmented-wave method, *Phys. Rev. B* **50**, 17953 (1994).
- [41] G. Kresse and D. Joubert, From ultrasoft pseudopotentials to the projector augmented-wave method, *Phys. Rev. B* **59**, 1758 (1999).
- [42] R. Armiento and A. E. Mattsson, Functional designed to include surface effects in self-consistent density functional theory, *Phys. Rev. B* **72**, 085108 (2005).
- [43] H. J. Monkhorst and J. D. Pack, Special points for Brillouin-Zone integrations, *Phys. Rev. B* **13**, 5188 (1976).
- [44] J. Heyd, G. E. Scuseria, and M. Ernzerhof, Hybrid functionals based on a screened Coulomb potential, *J. Chem. Phys.* **118**, 8207 (2003).
- [45] J. Heyd, G. E. Scuseria, and M. Ernzerhof, Erratum: “Hybrid functionals based on a screened Coulomb potential” [*J. Chem. Phys.* 118, 8207 (2003)], *J. Chem. Phys.* **124**, 219906 (2006).
- [46] G. A. Sai-Halasz, L. Esaki, and W. A. Harrison, InAs-GaSb Superlattice energy structure and its semiconductor-semimetal transition, *Phys. Rev. B* **18**, 2812 (1978).
- [47] R. Magri and A. Zunger, Effects of interfacial atomic segregation and intermixing on the electronic properties of InAs/GaSb superlattices, *Phys. Rev. B* **65**, 165302 (2002).
- [48] P. Piquini, A. Zunger, and R. Magri, Pseudopotential calculations of band gaps and band edges of short-period $(\text{InAs})_n/(\text{GaSb})_m$ superlattices with different substrates, layer orientations, and interfacial bonds, *Phys. Rev. B* **77**, 115314 (2008).
- [49] Y. Wei and M. Razeghi, Modeling of type-II InAs/GaSb superlattices using an empirical tight-binding method and interface engineering, *Phys. Rev. B* **69**, 085316 (2004).
- [50] W. M. Haynes, D. R. Lide, and T. J. Bruno, *CRC handbook of chemistry and physics* (CRC Press, Boca Raton, London, New York, 2016).
- [51] J. Wang, Y. Zhang, and L.-W. Wang, Systematic approach for simultaneously correcting the band-gap and p - d separation errors of common cation III-V or II-VI binaries in density functional theory calculations within a local density approximation, *Phys. Rev. B* **92**, 045211 (2015).
- [52] J. Wang and Y. Zhang, Band-gap corrected density functional theory calculations for InAs/GaSb type II superlattices, *J. Appl. Phys.* **116**, 214301 (2014).
- [53] A. P. Ongstad, R. Kaspi, C. E. Moeller, M. L. Tilton, D. M. Gianardi, J. R. Chavez, and G. C. Dente, Spectral blueshift and improved luminescent properties with increasing GaSb layer thickness in InAs-GaSb type-II superlattices, *J. Appl. Phys.* **89**, 2185 (2001).
- [54] R. Kaspi, C. Moeller, A. Ongstad, M. L. Tilton, D. Gianardi, G. Dente, and P. Gopaladasu, Absorbance spectroscopy and identification of valence subband transitions in type-II InAs/GaSb superlattices, *Appl. Phys. Lett.* **76**, 409 (2000).
- [55] J. Sun, A. Ruzsinszky, and J. P. Perdew, Strongly constrained and appropriately normed semilocal density functional, *Phys. Rev. Lett.* **115**, 036402 (2015).
- [56] See Supplemental Material at <http://link.aps.org/supplemental/10.1103/PhysRevApplied.18.024058> for more computing detail and results.
- [57] See Supplemental Material at <http://link.aps.org/supplemental/10.1103/PhysRevApplied.18.024058> for model structural file (VASP POSCAR format) in a separate zip file.